

## AN EXPERIMENTAL AND CFD STUDY OF A SUPERSONIC COAXIAL JET

A. D. Cutler\*

*The George Washington University, JIAFS, Hampton, VA*

J. A. White†

*NASA Langley, Hampton, VA*ABSTRACT

A supersonic coaxial jet facility is designed and experimental data are acquired suitable for the validation of CFD codes employed in the analysis of high-speed air-breathing engines. The center jet is of a light gas, the coflow jet is of air, and the mixing layer between them is compressible. The jet flow field is characterized using schlieren imaging, surveys with pitot, total temperature and gas sampling probes, and RELIEF velocimetry. VULCAN, a structured grid CFD code, is used to solve for the nozzle and jet flow, and the results are compared to the experiment for several variations of the  $\tilde{k} - \tilde{\omega}$  turbulence model.

NOMENCLATURE

$p_{amb}$	Ambient pressure
$p_{exit}$	Nozzle exit pressure
$p_{ref,CJ}$	Center-jet nozzle reference pressure
$p_{ref,coflow}$	Coflow nozzle reference pressure
$Pr_t$	Turbulent Prandtl number
$Sc_t$	Turbulent Schmidt number
$T_{amb}$	Ambient temperature
$T_{t,CJ}$	Center-jet nozzle total temperature
$T_{t,coflow}$	Coflow nozzle total temperature
$x$	Axial distance measured from center-jet nozzle exit plane
$y$	Radial distance
$\chi$	Mole fraction center-jet gas

INTRODUCTION

Computational fluid dynamics (CFD) codes are extensively employed in the design of high-speed air breathing engines. CFD based on the Reynolds averaged Navier-Stokes equations utilizes models for the turbulent fluxes which employ many ad hoc assumptions and empirically determined coefficients. Typically, these models cannot be applied with

confidence to a class of flow for which they have not been developed and tested. An experiment is conducted to provide data suitable for code development and testing. Results are compared to CFD solutions obtained by VULCAN, a previously developed code used in engine analysis.

The geometry chosen for the study is that of a coaxial jet discharging into stagnant laboratory air, with center jet of a light gas (a mixture of 5% oxygen and 95% helium by volume) and coflow jet of air. The exit flow pressure for both coflow and center-jet nozzles is 1 atmosphere. The presence of oxygen in the center jet is to allow the use of an oxygen flow-tagging technique (RELIEF<sup>2</sup>) to obtain non-intrusive velocity measurements. Both jets are nominally Mach 1.8, but because of the greater speed of sound of the center jet, its velocity is more than twice that of the coflow. The two stream mixing layer which forms between the center jet and the coflow near the nozzle exit is compressible, with an average of the calculated convective Mach number<sup>3</sup> of the center jet relative to the mixing layer and that of the mixing layer relative to the coflow,  $M_c$ , of 0.7.

This geometry has several advantages: The streamwise development of the flow is generally dominated by turbulent stresses (rather than pressure forces), and thus calculations are sensitive to proper turbulence modeling. It includes features present in supersonic combustors, including a high convective Mach number mixing layer near the nozzle exit, and a plume of light-gas/air mixture downstream. Since it is a free jet, it provides easy access for both optical instrumentation and probes. Since it is axisymmetric, it requires a minimum number of experimental measurements to fully characterize, and calculations can be performed with relatively modest computer resources. A disadvantage is that weak shock waves

\*Associate Professor, Senior Member AIAA

†Research Scientist, Senior Member AIAA

FLOW FIELD MEASUREMENTS

formed at the nozzle exit strengthen and turn normal as they approach the axis, complicating the flow. Care is thus taken in the design of the facility to provide as near as possible to 1-D flow at the exit of both center and coflow nozzles, and to minimize the strength of waves generated at the nozzle exit.

This experiment has been adopted by a working group of the NATO Research and Technology Organization as a test case for their CFD development and validation activity. Additional calculations have been presented,<sup>4</sup> using the SPARK code, and Cebeci-Smith turbulence model for the nozzle boundary layers and Eggars model for the jet mixing region.

FLOW FACILITY

The coaxial jet assembly is shown in Figure 1. It is axisymmetric and consists of an outer body and a center body. The passages formed by the space between these bodies, and by the interior passage of the center body, are nozzles designed by the method of characteristics to produce 1-D flow at their exit. Many details of this assembly have been previously described<sup>5,6</sup>.

The nozzle assembly is joined to the Transverse Jet Facility, located in the laboratories of the Hypersonic Airbreathing Propulsion Branch at NASA Langley Research Center. The plenum of this facility contains porous plates for acoustic dampening and screens for flow conditioning. Air is provided to the facility from a central air station, and the helium-oxygen mixture is provided to the center body from a bottle trailer containing premixed gas.

The assembly is instrumented with pressure taps: one in the center body just downstream of the screens, one in the facility plenum, and one in the outer body near the exit of the coflow nozzle (in a region where the flow has reached its exit condition). Thermocouples are located in the gas supply lines to measure supply temperature, and ambient (barometric) pressure and ambient temperature are read. The values of these various quantities during the probe surveys, and their respective uncertainties (95% probability band) are given in Table 1. Note that tabulated uncertainties are due to facility unsteadiness and variations in set point, and do not include  $\pm 0.5\%$  in pressures and  $\pm 2$  K in temperatures due to transducer error. Facility unsteadiness and set point errors are less than transducer errors for pressures. However, since air and helium-oxygen supply temperature are not controlled, set point errors are higher than transducer errors for temperature.

Various types of flow field measurement have been performed. The flow has been visualized with conventional schlieren and shadowgraph. Pitot, gas sampling, and total temperature probes have been employed to survey the flow. (Probe survey locations are listed in Table 2, and also shown in Figure 5.) References 5 and 6 give details of these measurements.

Survey probe tips are cylindrical and cut square, with outside/inside diameters respectively of the pitot probe 0.64 mm/0.36 mm, and of both the gas sampling probe and total temperature probe 1.27 mm/0.76 mm. The gas sampling probe and tubing internal diameters are sized to avoid choking the sample gas flow, ensuring shock attachment at the probe tip. The total temperature probe is a miniature shrouded, vented thermocouple. The probe incorporates a commercial microminiature thermocouple junction at the tip of a 0.20 mm diameter "needle". Errors in pitot pressure due to pressure transducer error are  $\pm 0.5\%$ . Error in total temperature due to thermocouple error is  $\pm 2$  K. In addition, the total temperature probe is found to read about 1% low, due to incomplete stagnation of the flow at the sensor and/or radiation losses.

The mole fraction of the center-jet gas (i.e., the He-O<sub>2</sub> mixture) in the gas withdrawn from the flow,  $\chi$ , is found in real time by a hot-film probe based system<sup>7</sup>. The largest contribution to the uncertainty of the system is the manufacturer-quoted  $\pm 1\%$  of full scale in the mass flow controller used to provide a helium-oxygen-air mixture to calibrate the system. Maximum uncertainty in mole fraction of helium-oxygen is in the range  $\pm 1-1.5\%$ , but uncertainty is less than this for mole fractions close to 0.0 or 1.0 where uncertainty in the composition of the calibration mixture approaches zero.

The probes were mounted in a diamond-airfoil strut, and translated in the flow by a two-component stepping-motor driven translation stage. Probe "zero" location was determined using machined fixtures mounted to the nozzle exit (conical extension cap removed). Surveys were conducted across a diameter of the flow. Analysis of the data to find the best-fit center showed it to be within 0.4 mm (95% of the time) of the measured center. Thus, probe surveys are taken to pass through the axis of the jet  $\pm 0.4$  mm. Survey data presented have been shifted (by less than  $\pm 0.4$  mm) so that the best fit center lies at  $y=0$ . Resulting data are found to be almost perfectly symmetrical.

In addition to these "conventional" techniques, the RELIEF<sup>1</sup> (Raman Excitation plus Laser-Induced Electronic Fluorescence) oxygen flow tagging technique has been used to provide measurements of

(instantaneous) axial component velocity. While these data have all now been acquired, they have not been fully analyzed, and will be presented at a future date.

### CALCULATIONS

The Favre-averaged Navier-Stokes equations are solved using VULCAN, a structured, finite-volume CFD code. The calculation assumes an axisymmetric flow of a mixture of thermally perfect gases: “air”, He and O<sub>2</sub>. Inviscid fluxes are calculated using the Kappa = 1/3<sup>rd</sup> MUSCL scheme with the approximate Riemann solver of Roe, while viscous fluxes are evaluated using 2<sup>nd</sup> order central differences. A diagonalized approximate factorization scheme is used for iterating the unsteady equations in pseudo-time to a steady-state solution. Coarse-to-fine-grid sequencing was used on three grid levels to accelerate the development of the solution.

The calculation was performed on a structured grid generated by a separate, commercial code. There are a total of 188,080 cells, distributed among five blocks, as illustrated in Figure 2. These blocks include three for the jet and surrounding flow (A, B, C), one for the coflow nozzle (D), and one for the center-jet nozzle (E). Grids are continuous at the block interfaces and, as may be seen in Figure 3, grid points are clustered near the walls of the nozzles to resolve the boundary layers, at the exit of the center-jet nozzle to resolve the recirculation zone and shocks in the vicinity of the nozzle lip, and to a lesser degree near the axis to resolve shock reflections. The distance from the wall of the centers of the closest cells is less than  $y^+ = 1.5$  on all surfaces.

The walls are specified to be adiabatic, and wall velocities are specified no slip. Total pressure and temperature conditions are specified at subsonic inflow/outflow planes, while the code switches to extrapolation where the code detects that outflow is supersonic. At the axis, an axisymmetric symmetry condition is applied. At the exterior boundary the composition is air with density of 1.177 kg/m<sup>3</sup> and pressure ( $p_{amb}$ ) 101.3 kPa. At the coflow nozzle inflow boundary the composition is air with total density 6.735 kg/m<sup>3</sup> and total pressure ( $p_{ref,coflow}$ ) 580.0 kPa. At the center-jet nozzle inflow boundary the composition is 0.7039 by mass He and 0.2961 by mass O<sub>2</sub> with total density 1.3343 kg/m<sup>3</sup> and total pressure 628.3 kPa (computed from  $p_{ref,CJ}$  and the area ratio between the reference plane and sonic throat, assuming quasi-1-D flow). Blocks A, B, and C are initialized with ambient air conditions and Blocks D and E are initialized with a quasi-1-D flow solution for the nozzles. Block C is then

overwritten by propagating (along grid lines) conditions from the block interfaces with D and E. Block A is then overwritten by propagating conditions from the block interface with C.

The flow is assumed to be turbulent, and variants of Wilcox's<sup>8</sup>  $\tilde{k} - \tilde{\omega}$  turbulence model are used: specifically, the high Reynolds number model, both with and without the compressibility correction proposed by Wilcox, and with and without Wilcox's generalization of Pope's modification to the  $\tilde{k} - \tilde{\epsilon}$  model, which attempts to resolve the “round jet/ plane jet anomaly”. In addition, calculations were performed using an explicit algebraic Reynolds stress model implemented in Wilcox's  $\tilde{k} - \tilde{\omega}$  model.<sup>9</sup> Turbulent Prandtl number and Schmidt number were set equal (the analogy between turbulent heat and mass transfer is stronger than the analogy between momentum and heat transfer), and varied in the range 0.75 to 1.0. The specific cases presented below are listed in Table 3. In column “Model”, B refers to the usual Boussinesq eddy viscosity approximation employed by Wilcox, and AS refers to the explicit algebraic Reynolds stress model. Column “Pope” refers to Pope's modification, and Column “Comp” refers to the compressibility correction.

The CFL number is ramped from 0.1 to 3.0 over a few thousand iterations at each grid level. Convergence on the fine grid is relatively slow, with about 30,000 iterations required to reduce the  $L_2$  norm of the residual 3.5 orders of magnitude, and most calculations are carried out to 40,000 or more iterations.

### RESULTS

Figure 4 is a typical schlieren image (with knife edge vertical) showing the jet with nozzle conical extension ring removed. Vertical dark and bright bands may be seen at the left and right edges respectively of the center jet, and also at the right and left edges of the coflow jet, due to large transverse gradients of refractive index. Notice also the shock/expansion wave structure emanating outward from the (0.25 mm thick) center-body lip. Similar waves propagate in the center jet, but are not visible in the schlieren due to the low refractive index there. The continuation of these initially inward propagating waves, after they have crossed at the axis and passed out of the center jet into the coflow air, is visible.

Figure 5 is a flooded contour plot of the Mach number from the CFD calculation (Case E). (Also shown are lines representing the data survey plane locations.) Mach numbers of 0.75 or below are

represented by black, and Mach numbers of 2.25 or above by white. Although the contour levels are not labeled, the results may be qualitatively compared to the schlieren. The waves seen radiating from the center-jet nozzle lip in the schlieren are found in the calculation, though are not fully resolved. A more detailed inspection shows that as the wave from the center-jet nozzle intersects the axis it forms a normal shock. This results in a slight deficit in pitot pressure at the axis, which is visible downstream of the shock in both CFD and experiment. This deficit persists as far downstream as  $x=100$  mm before it is obscured by the mixing of the coflow into the center jet.

Figures 6-9 show comparisons between the results of the experiment and the results of the CFD calculations for Case E, chosen because it gave the best results. Figures 10-15 show comparisons between the experiment and the CFD for various cases at Plane 14. The range of  $y$  in the plots does not correspond to the full range of the data or of the calculation, but is truncated to show more clearly the regions of interest. In these Figures,  $y$  is given in m.

It may be seen in Figure 6 that, proceeding downstream, the experimental  $\chi$  profile smoothly spreads, with the axis value falling below 1.0 downstream of about  $x=150$  mm. The experimental  $\chi$  is well reproduced by the calculation near the axis, but moving away from the axis the calculation is first high and then, near  $\chi=0$ , too low. Indeed, calculated  $\chi$  appears discontinuous in slope at  $\chi=0$  (a most unphysical behavior). Similar discontinuous slopes in velocity have been observed in calculations of (incompressible) wakes, jets and mixing layers using the  $k - \epsilon$  model, but not using the  $k - \omega$  model, in Reference 8.

The experimental pitot pressure at Plane 1, shown in Figure 7, reveals a layer of reduced pitot pressure, several times the thickness of the nozzle lip, separating the coflow and center jet. This layer results from the merging of the coflow nozzle inner surface and center-jet nozzle boundary layers with the small region of separation downstream of the lip. Small discrepancies between experiment and calculation in this layer may be experimental error associated with the effects of steep velocity gradient on the pitot probe, which is of significant diameter. Additionally, the flow in the center-jet nozzle may have been laminar or transitional, whereas the calculation assumed fully turbulent flow. Small axisymmetric irregularities visible in the experimental pitot pressure distribution in the center jet ( $-0.005$  m  $< y < 0.005$  m) may be attributed to small machining flaws in the center-jet nozzle. In general,

however, experiment and calculation agree very well, indicating that the calculations of the flow in the nozzles were good.

Pitot pressure results for several downstream planes are given in Figure 8. Agreement between experiment and calculation in the center jet is good except near the edge, where (as in the case of  $\chi$ ) spreading is underpredicted and calculated pitot pressure appears discontinuous in slope. Moving further out from the axis, a similar underprediction of the spreading rate of the mixing layer between coflow and ambient surrounding, and discontinuity in slope, may be seen.

Comparisons between experimental and calculated total temperature at Plane 9 (the only location this type of data were acquired) are shown in Figure 9. The experimental data at the axis and in the coflow are both about 1% below the known supply gas temperatures, due to previously discussed probe error. Moving out from the axis, the data initially rise above the center-jet supply gas temperature and then fall below the coflow jet supply gas temperature. In order to obtain the best agreement, this calculation used the experimentally measured supply gas temperatures of that particular run, rather than the average temperature over many runs, as used in all other calculations. (As may be seen in Table 1, gas supply temperatures varied substantially from run to run.) Given that the total temperature probe reads in error roughly 1% low, the calculation agrees well with the experiment, reproducing both overshoot and undershoot.

Figure 10 shows the pitot pressure for Cases A, C, and F at Plane 1, in the vicinity of (the wake of) the nozzle lip. Cases B, D, and E were omitted since there was no effect of the compressibility correction or of  $Pr_t$  and  $Sc_t$  at Plane 1 (they were the same as A). By comparison of A and C it may be seen that Pope's modification slightly reduces the wake width. Cases C and F, which utilized respectively the Boussinesq eddy viscosity approximation and explicit algebraic stress model, were almost identical. Note that there were no significant differences between any of the Cases in the freestream of either the center jet or coflow.

Figures 11 and 12 show the effect of Pope's modification and the compressibility correction on calculations utilizing the Boussinesq approximation for the eddy viscosity. The effect of the compressibility correction (compare B to A) on the spreading rate of the center jet is small, while it reduces the spreading of the mixing layer between coflow and ambient surroundings. The effect of the Pope's modification (C to A) is to reduce the spreading of both center jet and

coflow/ambient mixing layer.

Figures 13 and 14 show the effect of increasing the turbulent Prandtl and Schmidt numbers from 0.75 (E) to 0.9 (B) to 1.0 (Case D). The spreading of the center jet as seen in the profiles of  $\chi$  is reduced while the spreading as seen in profiles of pitot pressure is increased. In other words, the axis value of  $\chi$  is increased while the axis value of pitot pressure is reduced. There is of course, no effect on the coflow/ambient mixing layer.

Figures 15 and 16 compare the experimental data with the calculation using the explicit algebraic Reynolds stress model. In general, the calculation is similar to those performed using the Boussinesq approximation. Discontinuities at the boundary between the center jet and coflow, and the coflow and the coflow/ambient mixing layer are still present, although they seem a little less pronounced. The calculated  $\chi$  at the axis is a little low while the calculated pitot pressure is too low. The overall calculation might be improved by reducing  $Pr_t$  and  $Sc_t$  to 0.75, although center jet spreading would still be overpredicted.

**SUMMARY**

This paper describes an experimental and computational study of a flow with simple geometry, devised to test and develop turbulence models used in the analysis of scramjet combustors. The geometry is a coaxial nozzle producing a supersonic coaxial jet, with center jet helium. Various types of data have been acquired in the jet flow, including schlieren flow visualization, probe surveys, and RELIEF flow tagging velocity measurements. (The RELIEF data have not been presented, but will at a future date.) The series of calculations utilizes a structured finite difference code (VULCAN) and Wilcox’s  $\tilde{k} - \tilde{\omega}$  model, and considers the effects of and sensitivity to certain elements of the model. In particular, the compressibility correction, “Pope’s” modification, and the effect of turbulent Prandtl and Schmidt numbers are considered. In addition, an explicit algebraic Reynolds stress model utilizing the  $\tilde{k} - \tilde{\omega}$  model is tested. It was found that all models underpredicted mixing at the outer edge of the center jet and at the interface of the coflow with the coflow/ambient mixing layer, with severe discontinuities in slope of mole fraction center-jet gas and pitot pressure being observed.

**ACKNOWLEDGEMENTS**

The 1<sup>st</sup> author would like to acknowledge the support of the NASA Langley Research Center through

grant NCC1-370, and contributions by Dr’s G. S. Diskin and J. P Drummond.

**REFERENCES**

<sup>1</sup> White, J. A., Morrison, J. H., “A Pseudo-Temporal Multi-Grid Relaxation Scheme for Solving the Parabolized Navier-Stokes Equations,” AIAA Paper 99-3360, June 1999.  
<sup>2</sup> Diskin, G. S., “Experimental and Theoretical Investigation of the Physical Processes Important to the RELIEF Flow Tagging Diagnostic,” Ph.D. Dissertation, Princeton University, 1997.  
<sup>3</sup> Papamoschou, D., Roshko, A., “The compressible turbulent shear layer: an experimental study,” *J. Fluid Mech.*, Vol. 197, pp. 453-577, 1988.  
<sup>4</sup> Drummond, J. P., Diskin, G. S., Cutler, A. D., “Fuel-Air Mixing and Combustion in Scramjets,” Technologies for Propelled Hypersonic Flight, NATO Research and Technology Organization, Working Group 10, RTO Phase 1 Report EWP NR. 2122, Jan. 2001.  
<sup>5</sup> Carty, A. A., Cutler, A. D., “Development and Validation of a Supersonic Helium-Air Coannular Jet Facility,” NASA CR-1999-209717, Nov. 1999.  
<sup>6</sup> Cutler, A. D., Carty, A. A., Doerner, S. E., Diskin, G. S., Drummond, J. P., “Supersonic Coaxial Jet Experiment for CFD Code Validation,” AIAA Paper 99-3588, June 1999.  
<sup>7</sup> Cutler, A. D., Johnson, C. H., “Analysis of intermittency and probe data in a supersonic flow with injection,” *Experiments in Fluids*, Vol. 23, pp. 38-47, 1997.  
<sup>8</sup> Wilcox, D. C., *Turbulence Modeling for CFD*, 2<sup>nd</sup> Edition, DCW Industries, Inc., July 1998.  
<sup>9</sup> Abid, R., Rumsey, C. L., and Gatski, T. B., “Prediction of Nonequilibrium Turbulent Flows with Explicit Algebraic Turbulence Models,” *AIAA Journal*, Vol. 33, No. 11, 1995.

**TABLES**

$p_{ref,coflow}$ (kPa)	580 ± 2
$T_{t,coflow}$ (K)	300 ± 6
$p_{ref,C}/p_{ref,coflow}$	1.060 ± 0.008
$T_{t,C}/T_{t,coflow}$	1.02 ± 0.05
$p_{amb}/p_{ref,coflow}$	0.1758 ± 0.0012
$T_{amb}/T_{t,coflow}$	0.982 ± 0.017
$p_{exit}/p_{ref,coflow}$	0.1748 ± 0.0005

**Table 1 Experimental flow parameters.**

Number	$x$ (mm)
1	0.13
2	3.1
3	10.0
4	17.9
5	27.8
6	42.9
7	61.9
8	81.1
9	100.6
10	121.4
11	150.8
12	181.0
13	220.4
14	261.0

Table 2 Experimental survey locations.

Case	Model	Pope	Comp	$Pr_t, Sc_t$
A	B	Yes	Yes	0.9
B	B	Yes		0.9
C	B		Yes	0.9
D	B	Yes		1.0
E	B	Yes		0.75
F	AS		Yes	0.9

Table 3 CFD calculation cases.

FIGURES

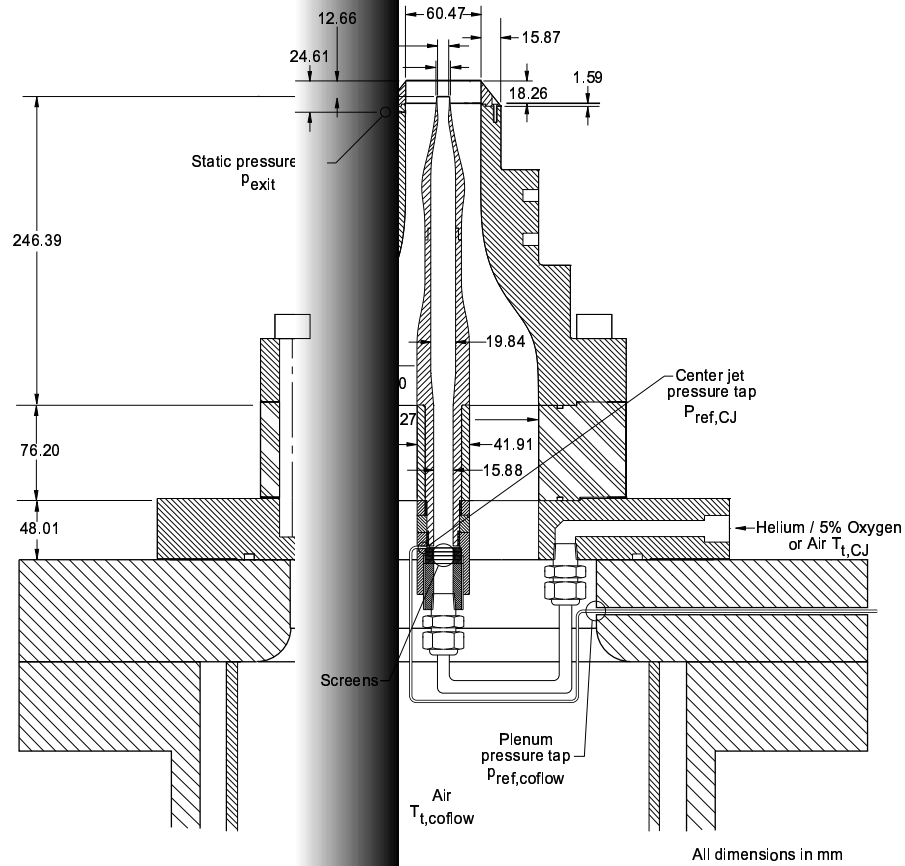


Figure 1 Coaxial jet assembly connected to Transverse Jet Facility.

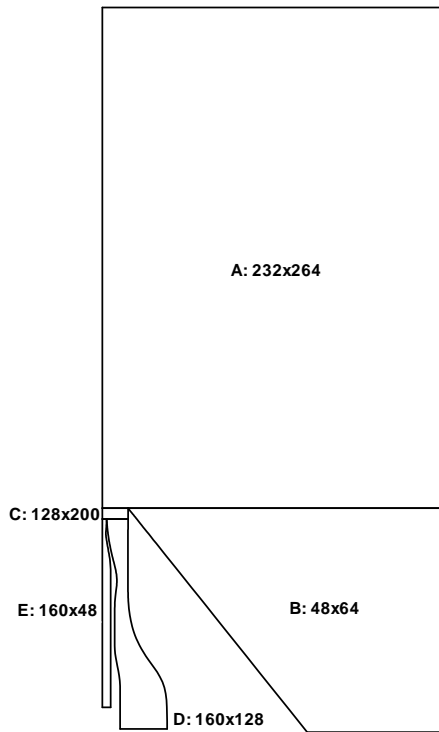


Figure 2 Computational blocks and numbers of cells ( $x \times y$ ).

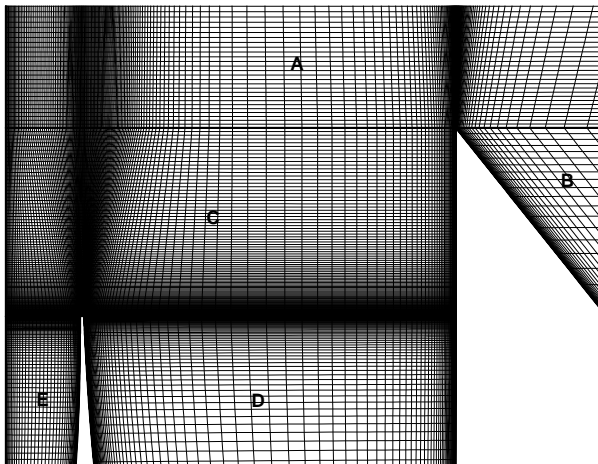


Figure 3 Detail showing grid lines in vicinity of nozzle exit.



Figure 4 Schlieren image with vertical knife edge (conical extension cap removed).

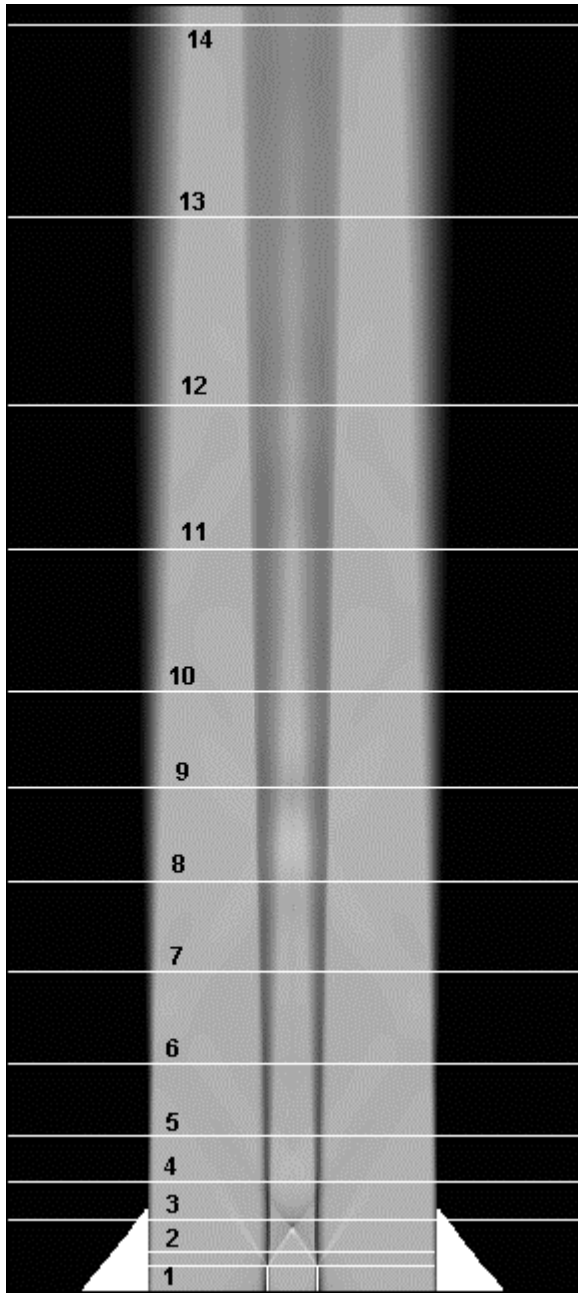


Figure 5 Calculated Mach number. Lines indicate data planes.

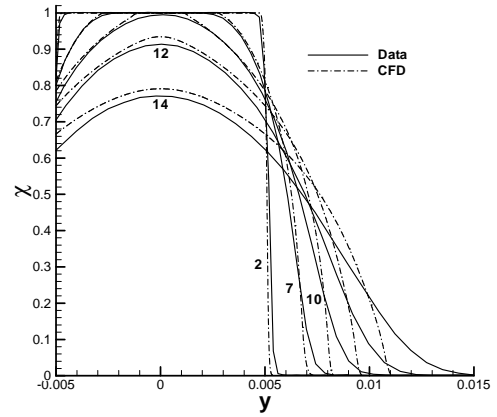


Figure 6 Mole fraction center-jet gas at several data planes: data versus CFD Case E.

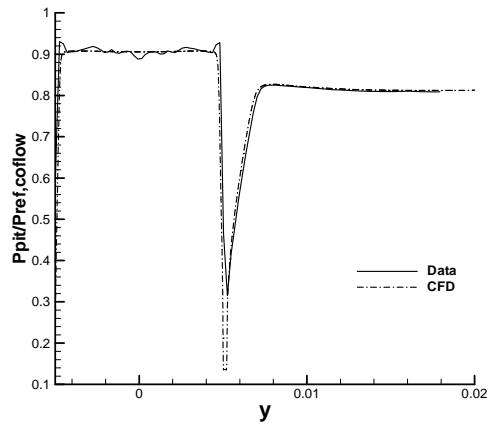


Figure 7 Pitot pressure at Plane 1: data versus CFD Case E.

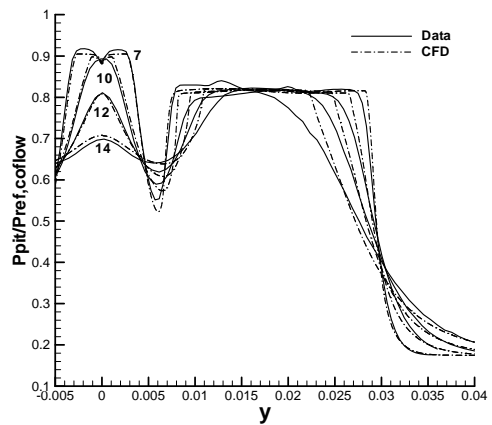


Figure 8 Pitot pressure at several planes: data versus CFD Case E.

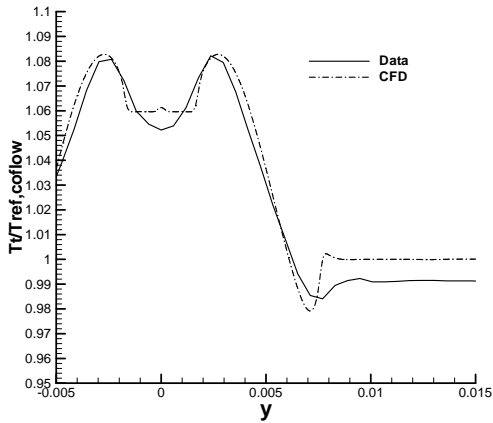


Figure 9 Total temperature at Plane 9: data versus CFD Case E.

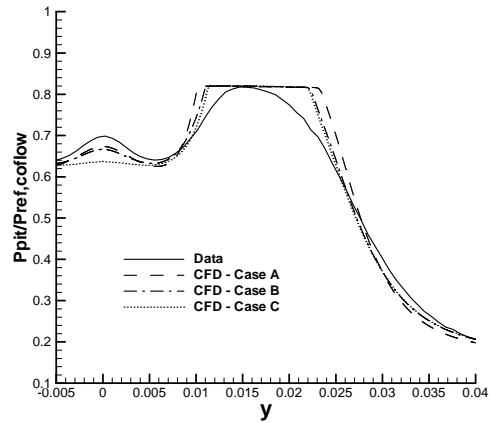


Figure 12 Pitot pressure at Plane 14: data versus CFD Cases A, B, C.

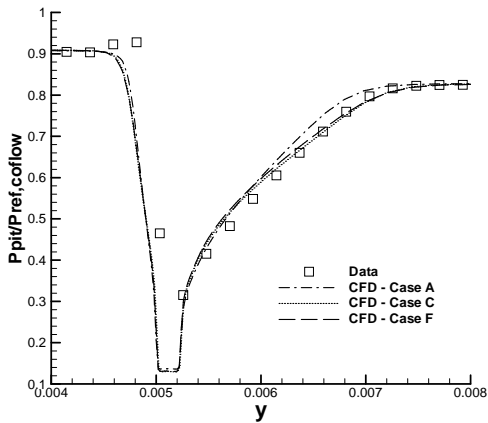


Figure 10 Pitot pressure at Plane 1: data versus CFD Cases A, C, F.

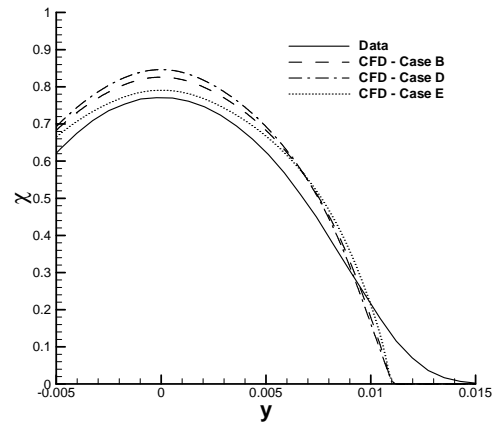


Figure 13 Mole fraction center-jet gas at Plane 14: data versus CFD Cases B, D, E.

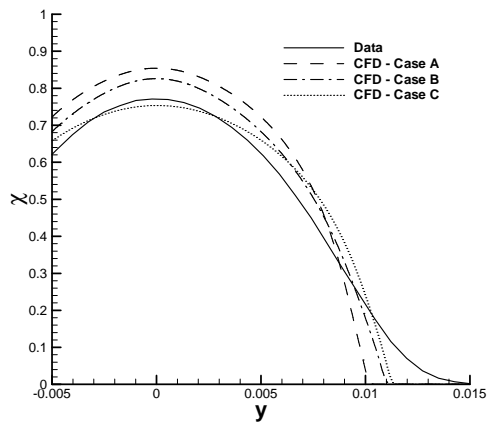


Figure 11 Mole fraction center-jet gas at Plane 14: data versus CFD Cases A, B, C.

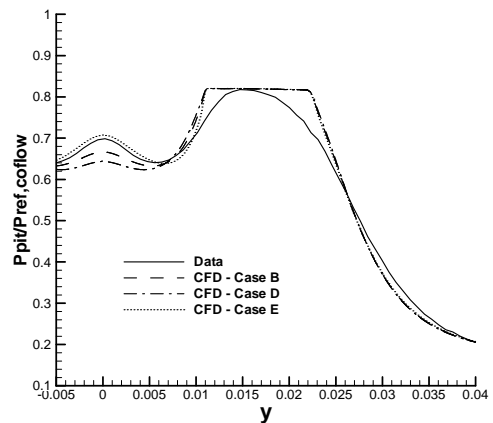
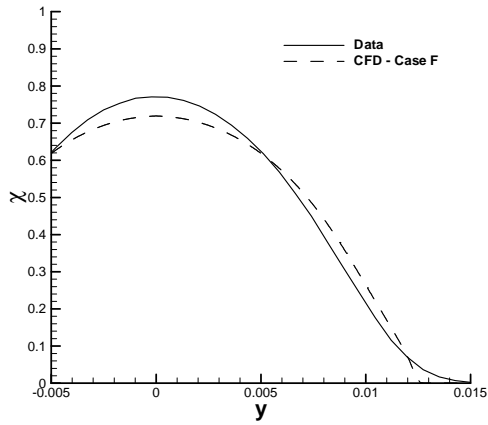
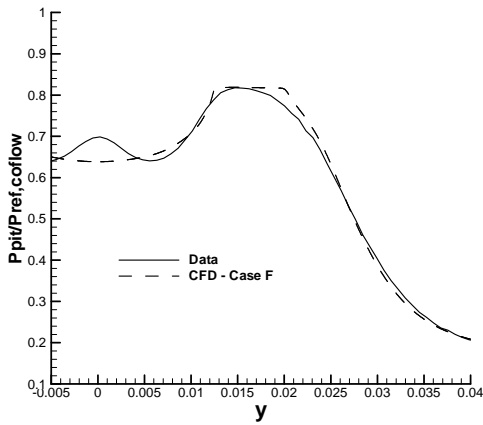


Figure 14 Pitot pressure at Plane 14: data versus CFD Cases B, D, E.



**Figure 15 Mole fraction center-jet gas at Plane 14: data versus CFD Case F.**



**Figure 16 Pitot pressure at Plane 14: data versus CFD Case F.**